Available online at www.sciencedirect.com

SciVerse ScienceDirect

Acta Materialia 61 (2013) 1383–1393

Acta MATERIALIA

www.elsevier.com/locate/actamat

Fatigue behavior of columnar-grained Cu with preferentially oriented nanoscale twins

Q.S. Pan, Q.H. Lu, L. Lu *

Shenyang National Laboratory for Materials Science, Institute of Metal Research, Chinese Academy of Sciences, Shenyang 110016, People's Republic of China

Received 29 September 2012; received in revised form 9 November 2012; accepted 12 November 2012
Available online 22 December 2012

Abstract

Polycrystalline columnar-grained bulk Cu samples containing preferentially oriented nanoscale twins have been synthesized by means of direct current electrodeposition. The *S–N* curves under tension–tension fatigue tests suggested that the fatigue limit ($\sigma_{max} = 162$ MPa at 10^7) of nanotwin Cu is greatly improved over that of the coarse-grained Cu with essentially a similar grain size ($\sigma_{max} = 110$ MPa at 10^7). It is found that the majority of twin boundaries are quite stable during cyclic deformation. Distinct "zigzag" slip bands acrossing a few twin planes are prevalently observed in the grain interiors. Schmid factor analysis shows that the "zigzag" slip bands result from one primary slip system activation of threading dislocations propagation within the twin lamellae, which is fundamentally different from that of polycrystal materials. The nanoscale twin confinement of activated threading dislocations suppresses the stress concentration, retards fatigue crack initiation and enhances the fatigue limit.

Keywords: Nanoscale twins; Fatigue behavior; "Zigzag" slip band; Dislocation structure; Copper

1. Introduction

Refining the grains of a material to enhance its strength has long been a strategy used in microstructure design. However, such beneficial effects of grain refinement are commonly accompanied by a reduction in ductility [1–5]. The limited ductility is ascribed to the significantly suppressed dislocation motion and accumulation to accommodate the plastic deformation in the limited space of nanometer-sized grains [1,5].

The fatigue limits of ultrafine-grained (UFG) and nanograined (NG) materials usually increase with decreasing grain size under high cycle fatigue (stress controlled), but they invariably exhibit a lower resistance to subcritical crack growth and a faster stable fatigue crack propagation rate in comparison to the conventional microcrystalline metals and alloys [6–10]. Because sub-micron-sized grains suppress the lattice dislocation activity, grain coarsening accompanied by shear band nucleation spread appears to sustain the cyclic plastic deformation during the fatigue process of UFG and NG materials [8,9,11]. The limited ductility, metastable microstructure and faster fatigue crack growth rate of UFG and NG materials greatly limit their engineering application because of safety concerns.

Over the past few years, attention has shifted to strengthening materials by means of engineering coherent twin boundaries (TBs) with low excess energy. Researchers have found that, by introducing a high density of nanoscale twins in the ultrafine-grained Cu sample, the strength of nanotwin Cu (nt-Cu) sample can be greatly enhanced, analogous to the strengthening of grain boundaries (GBs). Meanwhile, the ductility and work hardening of nt-Cu can still remain good [12–15]. The good combination of strength and ductility of nanotwin metals is ascribed to the unique barrier effect of TBs on the dislocation motion: the TBs not only serve as strong barriers in impeding the motion of dislocations, resulting in significant strengthen-

* Corresponding author. Tel.: +86 24 23971939; fax: +86 24 23998660.
E-mail address: llu@imr.ac.cn (L. Lu).

1359-6454/$36.00
http://dx.doi.org/10.1016/j.actamat.2012.11.015

ing similar to conventional GBs, but also possess more room for dislocation accumulation and storage, and improve ductility, which is fundamentally different from that of the conventional GBs [12–17]. Consequently, nanoscale TB strengthening is regarded as an effective strategy to improve strength while maintaining substantial plasticity to a large extent [5].

In spite of extensive studies of the TB strengthening mechanisms, including the experiments related to mechanical properties, such as strength, ductility and work hardening [12–15,18], plastic modeling [16,19] and simulations [20–24], the fatigue properties of twin structures are not well understood yet. Early research into twin structures focused on the fatigue cracking mechanisms near annealing TBs with the twin spacing in milli- or micrometer regimes. Thompson [25] found that TBs in pure Cu samples could serve as the potential sites for the initiation of fatigue cracks. Subsequently, Neumann et al. [26,27] observed that cracking occurred only at every other twin interface, which was proposed to result from the elastic anisotropy on both side of TBs, i.e. elastic incompatibility of TBs. Zhang et al. [28,29] indicated that, in coarse-grained (CG) Cu alloys, whether or not TB cracking occurs is intrinsically determined by the interactions between dislocations and TBs, which are controlled by the cooperative effects of the stacking fault energy (SFE), slip mode and crystallographic orientation in matrix and twins. As a systematic investigation in pure Cu, Cu–Al and Cu–Zn alloys, it is found that decreasing the SFE of Cu alloys will increase the number of dislocations piling up at TBs, finally initiating the fatigue cracks along TBs. Furthermore, the TB cracks also strongly rely on the difference of Schmid factors (DSF) on both sides of the twin plane. For a selected material, only when the DSF reaches a certain value will the TB fatigue crack mode occur. The two factors, SFE and DSF, are found to complement each other in facilitating TB cracking [29].

To date, only a few experimental fatigue studies have been carried out on nanotwin materials. For example, multilayer Cu/Cu thin film specimens containing aligned nanotwins introduced by magnetron sputtering deposition have shown a considerable microstructural stability and hardness retention under fatigue loading and indentation [30,31]. Both the fatigue limit (at 10^6) and the fatigue life of nt-Cu are much improved over that of CG-Cu. Detwinning appeared in some severely deformed columnar grains, followed by dislocation walls arising. The surface crack initiated from a surface depression, which is the intersection between a nanotwin column and an adjacent de-nanotwin column [30,31].

The twin lamellar thickness dependence of fatigue limit of pulsed electrodeposited nt-Cu foil was studied by cyclic tension–tension tests under stress control [32]. The results suggested that, with decreasing twin lamellar thickness, both the high fatigue life and the fatigue limit increase [32]. Moreover, increasing the twin density at a fixed grain size would not only be of benefit by increasing the fatigue limit, but would also enhance the fracture toughness, the threshold stress intensity factor range for fatigue fracture and the subcritical fatigue crack growth life [32,33].

The aforementioned studies on nanotwin materials were primarily carried out on foil or film samples. In this study, we performed traditional tension–tension fatigue tests on bulk Cu samples containing preferentially oriented nanotwins. The twin boundary stability and microstructural evolutions during the cyclic deformation process, including the slip morphology, crack formation and dislocation structure, were characterized by scanning electron microscopy (SEM), confocal laser scanning microscopy (CLSM) and transmission electron microscopy (TEM). A possible fatigue mechanism and the effect of twin components (TB orientation with respect to the loading direction, twin thickness and twin lamellar length, i.e. grain size) on cyclic deformation behavior of bulk nanotwin Cu samples are discussed.

2. Experimental

2.1. Sample preparation

High-purity copper sheets containing nanoscale growth twin lamellae were synthesized by means of a direct current electrodeposition technique from an electrolyte of $CuSO_4$. The $CuSO_4$ concentration was 90 g l^{-1} and the PH value was adjusted to ~1 with H_2SO_4. The soluble anode was made of a highly purified (99.995 wt.%) electrolytic copper sheet, while a pure Ti sheet with an exposure area of 20×40 mm^2 was used as the cathode substrate. By carefully controlling the deposition parameters during deposition, nt-Cu with a thickness of ~1.0 mm could be prepared. Details of the sample preparation procedure were described in Ref. [18]. For comparison, high-purity CG-Cu samples with essentially the same average grain size but with no significant density of twins were produced by annealing the cold rolling Cu samples at 200 °C for 2 h in air.

2.2. Tensile and fatigue tests

Dog-bone-shaped tensile and fatigue specimens with a gage section of 5×1.5 mm^2 were cut from as-deposited nt-Cu and CG-Cu sheets using an electrical spark machine. They were then mechanically polished to a final thickness of ~500 μm from the growth surface. Before tensile and fatigue testing, all specimens were electropolished in a solution of phosphoric acid (25%), alcohol (25%) and deionized water (50%) at ambient temperature to minimize the surface roughness and produce a strain-free surface for microstructural observation. Uniaxial tensile tests were performed in an Instron 5848 microtester at a strain rate of 6×10^{-3} s^{-1}. A contactless MST LX300 laser extensometer was used to calibrate and measure the strain of the samples upon loading.

Cyclic tension–tension tests were performed on an Instron E1000 testing machine under stress control with a

stress ratio r (r is defined as $\sigma_{max}/\sigma_{min}$) of 0.1 and a sinusoidal wave with a frequency of 30 Hz at room temperature. The fatigue limits of the as-deposited nt-Cu and CG-Cu were tested strictly by the staircase method [34]. Stress increments were taken to be ~5% of the initial estimate of the mean fatigue limit [34].

2.3. Microstructure characterization

The plane-view and cross-section microstructures of nt-Cu specimens before and after fatigue tests, which are defined as observations of the top growth surface and the side surface perpendicular to the top surface, respectively, were characterized in a FEI Nova NanoSEM 430 field emission gun scanning electron microscope with backscattered electron imaging using a VCD detector. The plane-view slip morphologies and fracture surface of as-fatigued specimens were examined by SEM with secondary electron imaging using an Everhart–Thornley detector. Three-dimensional (3-D) surface slip morphologies of the as-fatigued nt-Cu specimens were investigated by CLSM (Olympus LEXT OLS4000) with a planar resolution (namely, in the x–y plane) of 120 nm and a height resolution (along the z-axis) of 10 nm.

The cross-section microstructures of both as-deposited and as-fatigued nt-Cu specimens were characterized by using a JEOL 2010 transmission electron microscope operated at 200 kV. Cross-sectional TEM foils were sliced parallel to the cyclic loading axis with an electrical spark machine and mechanically polished to a final thickness of ~40 μm. After being punched, the TEM foils were fixed to 3 mm diameter Cu rings with a hole of diameter 0.5 mm and thinned by twin-jet polishing in an electrolyte of phosphoric acid (25%), alcohol (25%) and deionized water (50%) at −10 °C.

3. Results

A plane-view SEM image of the as-deposited columnar-grained nanotwin Cu, hereafter referred as to col-nt-Cu, reveals that polycrystalline grains are roughly equiaxed, as shown in Fig. 1a. Statistical distribution of grain size shows that the grain size ranges between 1 and 20 μm with an average value of ~6 μm (Fig. 1d). Some straight interfaces can be found clearly in a few grains. Further cross-section SEM observation shows that most grains are in the columnar shape with an average length of ~40 μm. TEM images confirm that high densities of parallel growth twin lamellae, most of which are predominantly normal to the growth direction, are embedded within the columnar grains (Fig. 1b and c). Occasionally, some twin lamellae inclined to the growth direction are found in a few columnar grains. Statistical results of twin thickness (λ) from amounts of TEM images reveal a broad distribution from several nanometers to ~400 nm with an average twin thickness of 78 nm (Fig. 1e). EBSD analysis confirmed that a strong (1 1 1) out-of-plane texture exists in the as-deposited Cu samples.

For comparison, plane-view and cross-section SEM observations were also performed on CG-Cu samples. It demonstrated that the grains are roughly equiaxed in three dimensions without significant density of twins. Statistical measurement shows that CG-Cu has an average grain size of 7 μm, essentially similar to that of the col-nt-Cu sample.

Typical tensile engineering stress–strain curves of col-nt-Cu and twin-free CG-Cu with essentially similar average grain size are shown in Fig. 2. Apparently, nanoscale twins

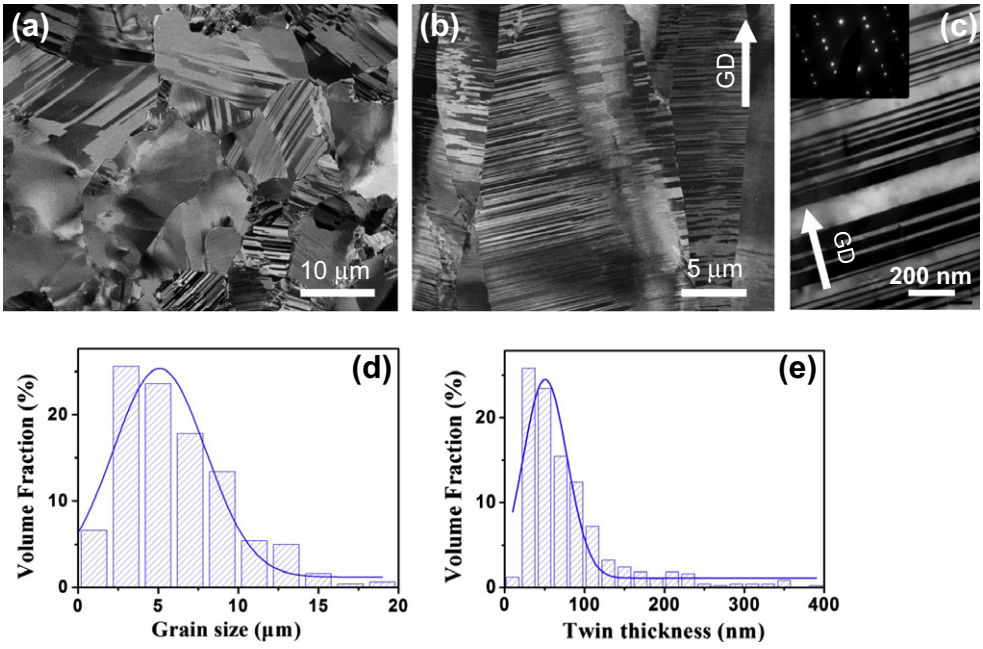

Fig. 1. SEM images of the as-deposited columnar nanotwin Cu sample from (a) the plane view and (b) the cross-section view. (c) Cross-section TEM image. (d) The grain size distribution and (e) the twin thickness distribution for as-deposited col-nt Cu sample. GD is the growth direction.

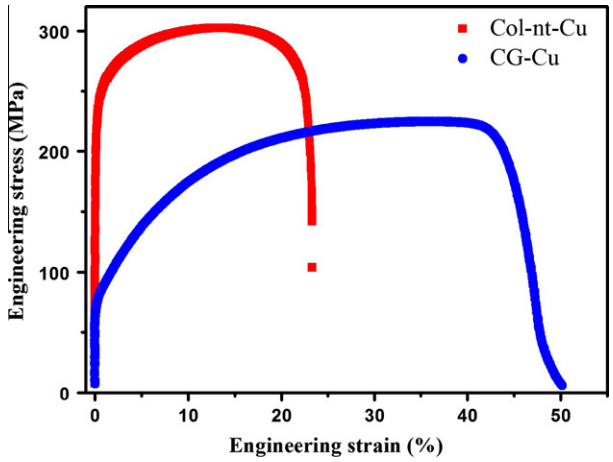

Fig. 2. Tensile engineering stress–strain curves of as-deposited col-nt-Cu and twin-free CG-Cu with the comparative grain size.

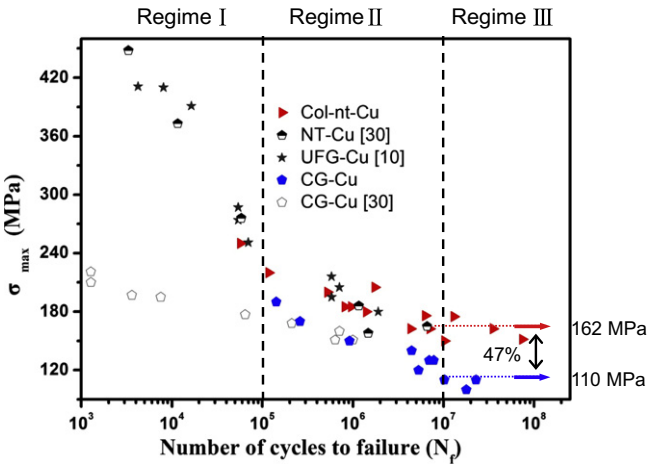

Fig. 3. Dependence of the fatigue life (N_f) on the cyclic maximum stress for col-nt-Cu and twin-free CG-Cu. Literature data obtained at a frequency of 10 Hz are included for comparison [10,30].

embedded within columnar grains play an important role in tensile behavior of col-nt-Cu. The col-nt-Cu displays a yield strength (σ_y, at 0.2% offset) of 225 MPa and an ultimate tensile strength (σ_{uts}) of ~300 MPa, much higher than that of the twin-free CG-Cu. In addition, col-nt-Cu also exhibits a considerable tensile uniform strain δ_u of 14% and elongation-to-failure of 26%, respectively. Table 1 summarized the microstructural characteristics and mechanical properties of col-nt-Cu and CG-Cu specimens.

The dependence of the fatigue life N_f on cyclic maximum stress for both col-nt-Cu and twin-free CG-Cu is shown in Fig. 3. It indicates that both the fatigue life and the fatigue stress of col-nt-Cu are improved relative to twin-free CG-Cu simultaneously. Even at the lower stress range, the difference in the fatigue life can be seen clearly. For example, the fatigue life of col-nt-Cu lasts at least 10 million cycles longer than that of CG-Cu at a maximum stress of 162 MPa. The difference in fatigue life for both materials is also obvious at high stress range.

The increment in fatigue stress of col-nt-Cu is different at different fatigue life regimes. Similar trend is also found in the *S–N* curve of the UFG-Cu samples [10] and sputter-deposited nanotwin Cu films [30]. According to the stress difference between these materials, the *S–N* curves in Fig. 3 can be divided into three regimes: Regime I (low cycle fatigue with $N_f < 10^5$), Regime II (medium cycle fatigue with $10^5 < N_f < 10^7$), Regime III ($N_f > 10^7$, known as the fatigue limit regime). Obviously, the difference between the cyclic maximum stress of Cu samples with nanostructures (both nanocrystals and nanotwins) and that of CG-Cu at a given fatigue life is most obvious in Regime I. A minor gap in the cyclic maximum stress was observed at a given life in Regime II. In Regime III, the fatigue limit of columnar-grained nt-Cu is $\sigma_{max} = 162$ MPa, which is 47% higher than that of the CG-Cu counterpart ($\sigma_{max} = 110$ MPa). This suggests that a high density of nanoscale twins can considerably improve the fatigue limit of microsized bulk Cu samples, analogous to that observed in NG materials.

Microstructures of the as-fatigued col-nt-Cu samples were systematically investigated by SEM, CLSM and TEM, respectively, from different directions, as schematically illustrated in Fig. 4a. In comparison with the glossy surface in the col-nt-Cu sample before fatigue, a typical surface morphology with two sets of mutually orthogonal slip features was observed on the top surface of the fatigued specimen at a maximum cyclic stress σ_{max} of 225 MPa, as shown in Fig. 4b. Statistical results show that traces of slip bands were predominantly distributed at an angle of ~±45° with respect to the cyclic loading axis. Generally, one set of parallel traces of slip bands was detected in individual grains with deformation features, indicating that only one primary slip system was preferentially activated in single grain.

The 3-D plane-view traces of slip bands in the fatigued col-nt-Cu were studied by the CLMS technique from the top surface (as schematically shown in Fig. 4). Many slip-induced "hill" and "valley" shapes with an angle of 45° relative to the loading axis are observed in Fig. 4c. The depth

Table 1
Summary of the microstructural characteristics and tensile properties of col-nt-Cu and twin-free CG-Cu.

Sample	d (μm)	λ (nm)	σ_y (MPa)	σ_{uts} (MPa)	ε_u (%)	ε_f (%)
col-nt-Cu	6	78	225 ± 10	303 ± 10	13.6 ± 0.6	25.8 ± 2.1
CG-Cu	7	–	85 ± 6	231 ± 7	35.1 ± 1.8	47.3 ± 2.0

d is the average grain size; λ is the average twin thickness; σ_y is the 0.2% offset yield strength; σ_{uts} is the ultimate tensile strength; δ_u is the uniform strain; δ_f is the strain to failure.

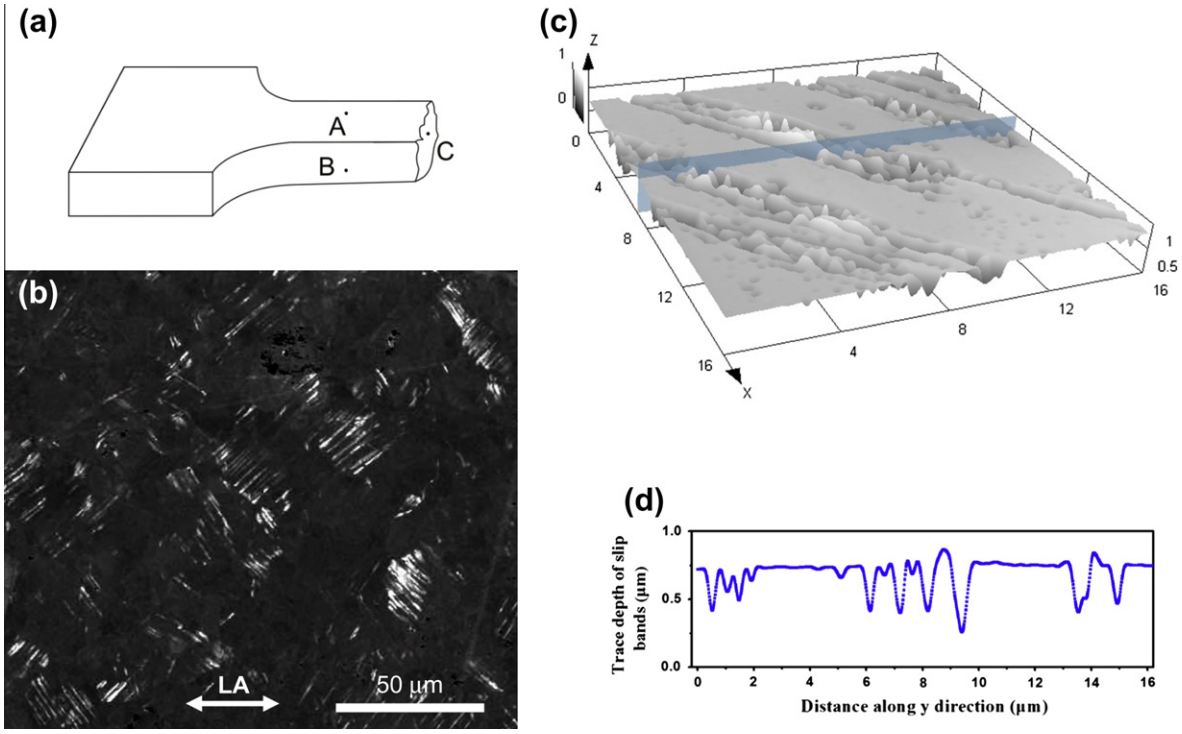

Fig. 4. (a) Schematic illustration of microstructural observation in different directions for col-nt-Cu sample fatigued at a maximum cyclic stress of 225 MPa. The *A* direction is from the top surface, i.e. a plane-view observation; *B* is from the side perpendicular to the top surface, i.e. a cross-section observation; *C* is from the fracture surface. (b) A typical plane-view SEM image showing slip band traces. (c) Plane-view CLSM observation showing 3-D slip morphologies. (d) "Hill" and "valley" shapes of plane-view traces of slip bands in a grain surface. LA denotes the cyclic loading axis.

of the "valley" is clearly generally larger than that of the "hill" (Fig. 4d), which is distinct from the dominant extrusion morphology observed in fatigued CG-Cu [35–37]. The depth of the "valley" ranges from 50 to 550 nm, which is comparable to the twin lamellar spacing distribution, as shown in Fig. 1e.

The microstructures of the as-fatigued col-nt-Cu with different local cumulative cyclic strains were investigated by SEM observations from the B direction (Fig. 5). The original TBs and GBs in the fatigued samples can be distinguished clearly. For the grains undergoing a relative smaller strain, this shows that the strain was undertaken by a few typically long slip bands, most of which are parallel to each other and can be seen to spread across a number of TBs in an individual columnar grain (Fig. 5a). The slip band could move either tens of micrometers (with slip across hundreds of twin planes) or just a few micrometers. High-magnification SEM observations (Fig. 5b) indicated the line-like slip morphology changes into a long "zigzag" slip band crossing a number of nanoscale twin lamellae. The slip band would change its slip direction when encountering TBs due to crystallographic symmetry on both sides of TBs. The change in slip direction is distinct in wider twin lamellae, but becomes indistinguishable in thinner twin lamellae in Fig. 5b. It is noted that the slip behavior was not observed throughout all columnar grains, although a strong (1 1 1) out-of-plane texture exists in col-nt-Cu samples.

A very rough surface morphology with more "zigzag" slip bands is observed universally in the columnar grains at a large strain, as shown in Fig. 5c. This indicates the presence of "zigzag" slip bands in grains bearing a large local cumulative cyclic strain. Most of the "zigzag" slip bands are still roughly parallel to each other, though a few are not, probably due to severe slip activities. The original TBs and GBs in the fatigued col-nt-Cu samples could not be distinguished easily. In order to explore the origination of the "zigzag" slip bands, the top surface of the cross-section side of fatigued col-nt-Cu samples was mechanically polished, showing that TBs are still visible, and then cut into a number of mini-blocks of sub-micrometer to micrometer size. The block size along the twin direction shows an average value of ~1 μm (Fig. 5d). The obvious contrast between the neighboring blocks may be caused by the residual dislocations in different positions of one twin lamellar interior.

The cross-section surface of the as-fatigued col-nt-Cu before polishing can also be observed by the 3-D CLSM technique, as shown in Fig. 6a. Slip bands are almost distributed homogeneously, with many sharp "hills" and "valleys" of slip steps, even in one twin lamella, which are different from the extrusions with a rough profile observed in fatigued CG-Cu [35]. The height of the slip steps, defined as the altitude difference between an adjacent "hill" and "valley", shows a wide distribution from 60 to 730 nm, which is slightly smaller than the reported average extrusion height (500–1000 nm) of CG-Cu samples [38–40]. This means that the dislocation slipping behavior in grain interiors was well confined, due to the presence of nanoscale twins in col-nt-Cu. The statistical

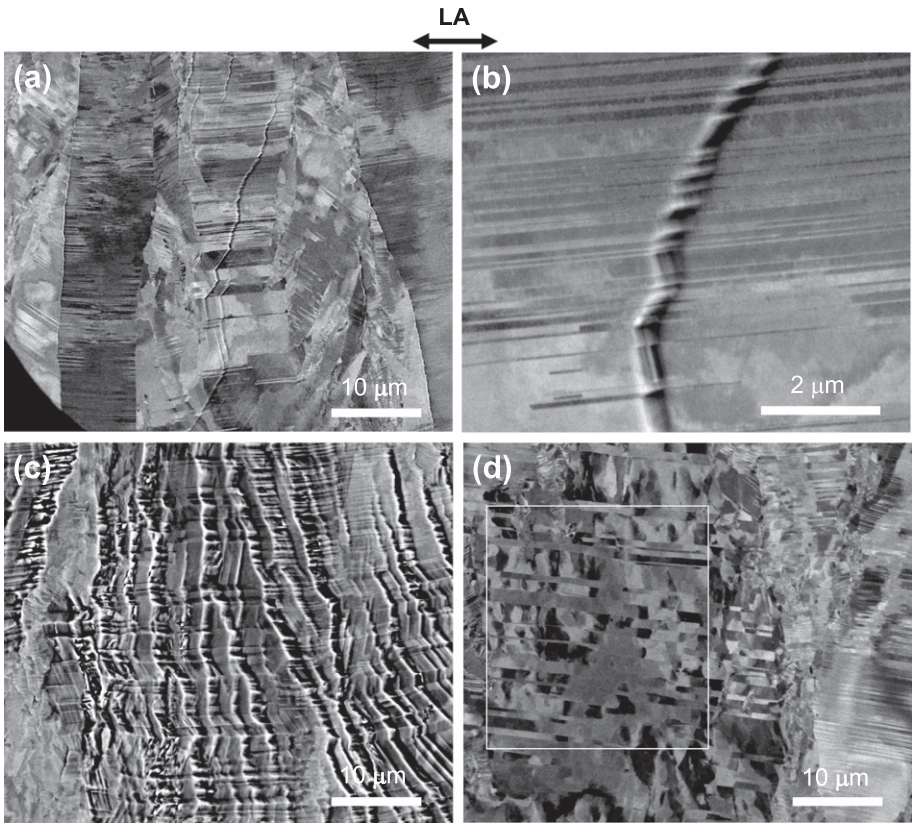

Fig. 5. Typical cross-section SEM images showing "zigzag" slip bands crossing TBs in columnar grains: (a) at a small cumulative plastic strain; (b) a magnified view of (a); and (c) at a larger cumulative plastic strain. (d) Cross-section SEM image showing block structures intersecting twin boundaries in grain interiors for col-nt-Cu fatigued at 225 MPa maximum stress, after surface polishing.

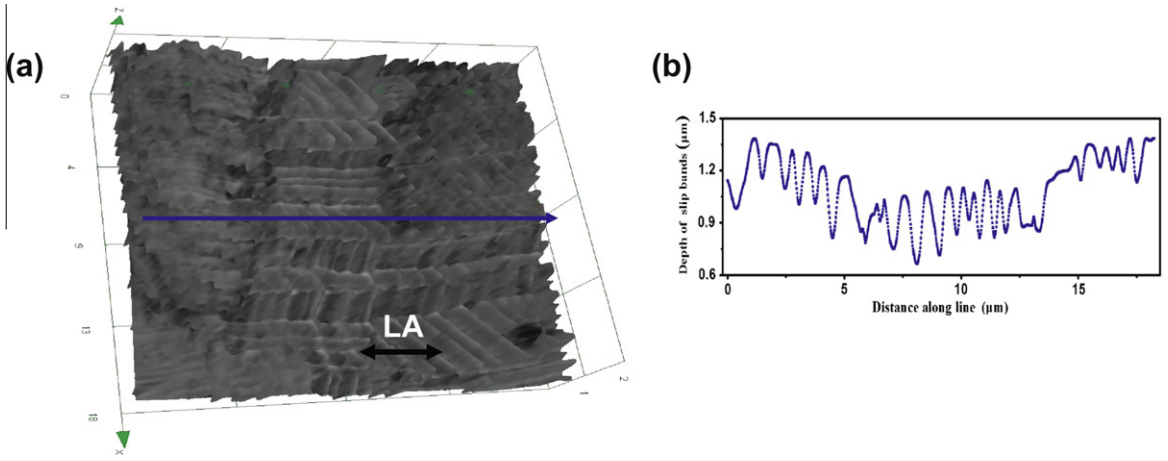

Fig. 6. (a) Cross-section CLSM observation showing the 3-D morphology of "zigzag" slip bands for col-nt-Cu fatigued at a maximum cyclic stress of 225 MPa. (b) Feature of slip steps produced by dislocations sliding in twin lamellar interiors.

analysis showed the average spacing between adjacent slip bands, i.e. the horizontal distance between an adjacent "hill" and "valley" of the slip steps, is ~0.9 μm, comparative to the size of blocks along TBs (Fig. 5d).

Fracture surface of the fatigued co-nt-Cu samples studied by SEM from the C direction is shown in Fig. 7a. Many columnar grains are clearly identified on fracture surface. Mini-cracks were observed at the GBs of columnar grains, as indicated by the arrows in Fig. 7a. Typical "zigzag" slip morphologies in the columnar grain interiors are detected on the fracture surface at a higher magnification (Fig. 7b), bearing a strong resemblance to the SEM observations of fatigued col-nt-Cu specimens from the B direction (Figs. 5a–c and 6a).

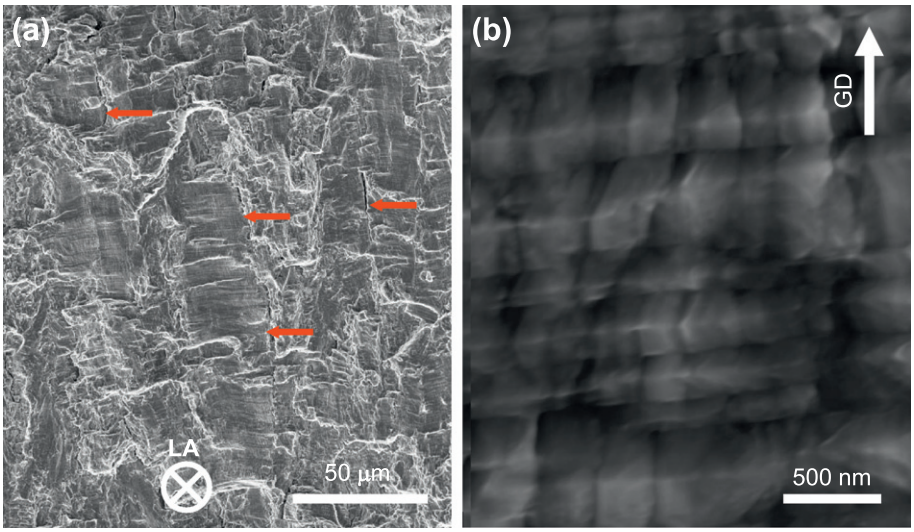

Fig. 7. SEM observations of the fracture surface from the *C* direction for col-nt-Cu sample fatigued at a maximum cyclic stress of 225 MPa. (a) Many columnar grain morphologies and mini-cracks at GBs. (b) "Zigzag" slip morphologies in grain interiors. The circle with a cross denotes the imposed cyclic loading axis perpendicular to the fracture surface.

4. Discussion

The cyclic deformation of the conventional polycrystalline CG-Cu is dominated by the dislocation activities. In the interior of the individual grain, single-slip-induced dislocation structures, such as persistent slip bands (PSBs) with a ladder structure and veins composed of densely packed dipoles, are frequently observed under low cyclic stress or strain, while multiple-slip-induced labyrinth structures and dislocation cells are found under high cyclic stress or strain [36,41–44]. Generally, in the grains with single slip, PSBs nucleate by breaking up of the veins at their edge, followed by dynamic rearrangements of dislocation dipoles [45,46]. After nucleation of PSBs, static extrusions formed rapidly by emergence of interfacial dislocations (including dipole activity associated with the production of vacancies), and their surface was gradually roughened by random irreversible slip [46–49]. The extrusions (accompanied by intrusions) related to the dislocation activity would act as the crack initiation sites [35,48,49]. Extrusions are usually the dominant feature on the top surface for cyclic deformed single-crystal and polycrystalline face-centered cubic (fcc) metals from a macroscopic view.

In the present study, however, the extrusions are very limited in fatigued col-nt-Cu, either from the top surface or from the side surface. The cyclic deformation of the columnar-grained Cu with nanoscale twins is still governed by the dislocation activities, as suggested by Figs. 4 and 5, but no PSB-related ladder structures or labyrinth/cells structures are observed. Typical traces of slip bands with an angle of 45° with respect to the cyclic loading axis are dominant on the top surface. Simultaneously, zigzag-shaped slip bands crossing TBs are extensively seen from the side perpendicular to the top surface, which suggests that the cyclic deformation mechanism of the col-nt-Cu is governed by a different cyclic mechanism.

In order to explore the intrinsic deformation mechanism of the columnar-grained Cu with preferentially oriented nanotwins under cyclic tension–tension tests, the Thompson tetrahedron notation is used to consider the most possibly activated slip systems in nt-Cu crystal. Fig. 8a shows the pair of Thompson tetrahedra corresponding to the original fcc and twinned fcc crystals. The four vertices of the tetrahedron are labeled A, B, C and D. Symbols with a superscript T represent objects in the twin orientation. The mirror (twin) plane is the hatched ABC plane. The upper and lower Thompson tetrahedra, i.e. ABCD and $A^TB^TC^TD^T$, illustrate the slip systems of crystals M and T in the notation of Fig. 8a. Owing to the mirror symmetry of slip systems, 12 physically distinct slip systems in the twin layer are considered in the present study.

Based on the orientations of the slip plane and the Burgers vector relative to the twin plane, the 12 slip systems can be classified into three categories:

- *Hard mode I*: both the slip plane and the slip direction of the active slip system are inclined to TBs. In this case, dislocations will pile up against and slip across the TBs.
- *Hard mode II*: the slip plane is inclined to TBs, but the slip direction is parallel to them. In this case, dislocations will not pile up against the TBs; instead, they will bow out, like the threading dislocations observed in nanoscale thin films and multilayer materials [18,50–52], through channels confined by neighboring TBs.
- *Soft mode III*: both the slip plane and the slip direction are parallel to TBs. It is mostly Shockley partial dislocations that are nucleated and propagated along the TBs.

On the basis of the above analysis, we calculated the Schmid factor of the 12 slip systems to analyze the primary slip system preferentially activated in twin lamellar interiors. Considering the microstructural complexity in our

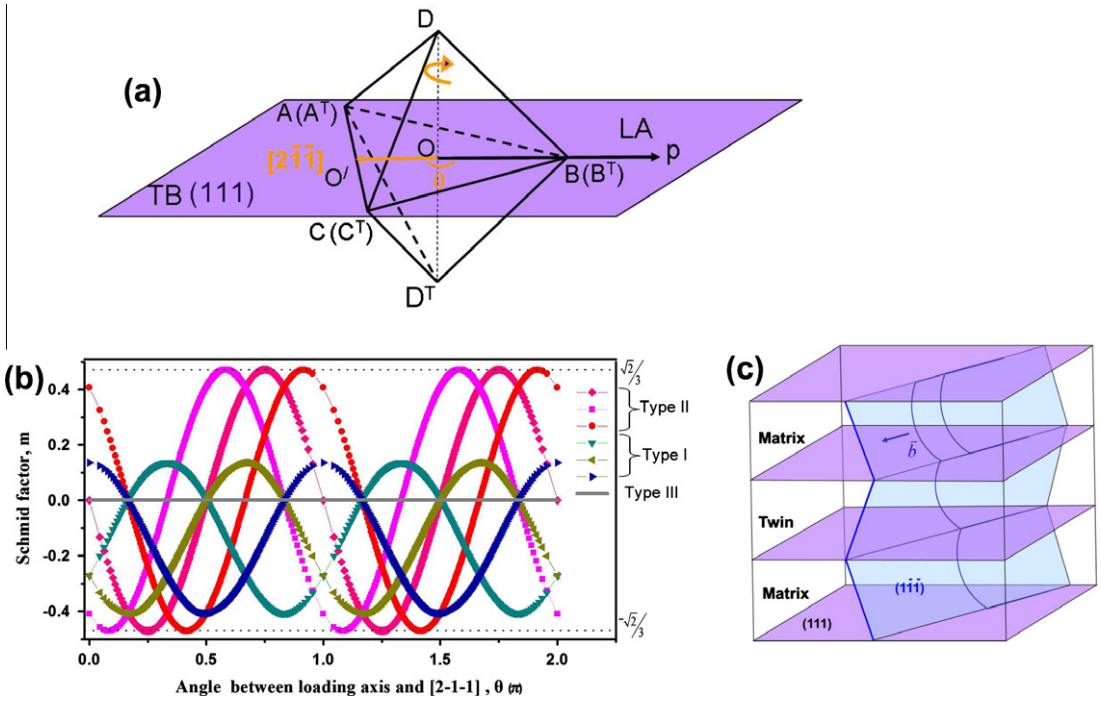

Fig. 8. (a) Schematic illustration of a double Thompson tetrahedra rotating around axis DD^T on the coherent TB, i.e. the (1 1 1) slip plane, for the overwhelming majority columnar grains with nanoscale twin lamellae parallel to the imposed cyclic loading axis. (b) Variation in the Schmid factors of 12 slip systems as a function of rotation angle θ. (c) Schematic illustration of the activated threading dislocations in adjacent twin lamellae.

samples, the in-plane crystallographic orientation, i.e. the orientations of double Thompson tetrahedra in different columnar grains, is randomly distributed relative to the applied cyclic loading axis. To explain this scenario, we suppose that the pair of Thompson tetrahedra with a coherent TB could rotate around the axis DD^T while the applied cyclic loading axis is fixed parallel to the horizontal direction. In order to express the in-plane orientation of Thompson tetrahedra relative to the imposed loading axis, the rotation angle θ, ranging from 0 to 2π, is defined as the angle between oo' and the applied cyclic loading axis OP. The variation of the Schmid factors of the 12 slip systems as a function of the rotation angle θ is illustrated schematically in Fig. 8b. According to the above analysis, the alignment of the cyclic loading axis parallel to TBs makes the Schmid factor of the soft mode III zero (Fig. 8b). This means that the nucleation and movement of partial dislocations along the twin plane are impossible.

The Schmid factor of the slip systems belonging to hard mode I is also relatively smaller than that of the hard mode II slip system for grains with any in-plane orientation. Therefore, the hard mode II, with threading dislocations propagating through confined neighboring nanoscale twin channels are preferentially activated (Fig. 8c). This result accords with the results of tensile and compression tests, in which the loading axis is parallel to the majority of the twin planes. You et al. [18] verified that the effective confinement of threading dislocation slip inside the lamellar channels dominates plastic deformation in twin interiors. Hard mode II slip systems with threading dislocations are activated and result in strengthening by the confined layer slip (CLS) mode, where the strength is proportional to $1/\lambda$. Therefore, the result shows that the CLS mode, which was originally postulated for the confined dislocation slip in nanoscale thin layers, can also explain the obvious fatigue limit difference between col-nt-Cu and CG-Cu in Regime III in Fig. 3. However, the similarity between the *S–N* curves for the fatigued nanotwin Cu and for UFG Cu is beyond our current understanding (this is a work in progress).

Since crystallographic symmetry exists on both sides of the twin plane, alignment of the cyclic loading axis parallel to the TBs leads to the slip system being activated in two adjoining twin lamellae that are symmetrical relative to the twin plane. Therefore, the active threading dislocations in the individual grain belong to one slip system during cyclic loading. In this case, the threading dislocations in two adjacent twin lamellae will shear a segment at TBs and propagate through the twin lamellar channel in one direction, which is in a lower energy state (Fig. 8c).

TEM observations from the perpendicular direction to the top surface in the as-fatigued sample confirmed that a large amount of threading dislocation arrays spanned the adjacent TBs (Fig. 9a). Comparison with the as-deposited microstructure, the majority of TBs in the grain interior are still visible, though many defects are found at the twin lamellar interiors and at TBs. The TBs are intact, straight and parallel to each other, indicating that the majority of them are quite stable during cyclic deformation. Very little detwinning and extended dislocation walls are seen in the

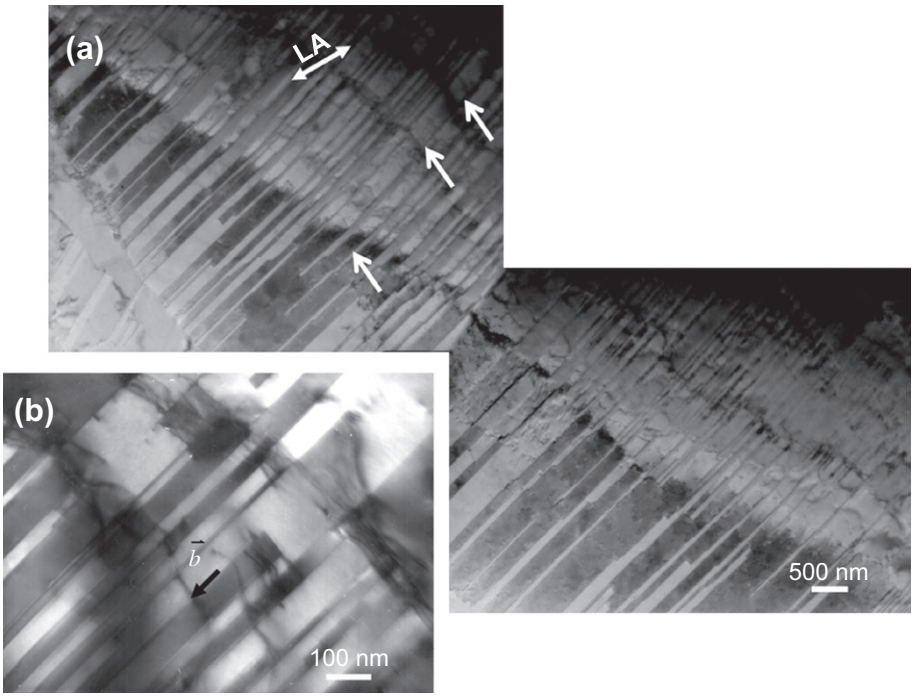

Fig. 9. Cross-section TEM images for col-nt-Cu sample fatigued at a maximum cyclic stress of 225 MPa. (a) The majority of TBs are straight and intact, and many dislocation arrays stride TBs. (b) Bundles of dislocation lines are confined by a few adjacent TBs. The Burgers vector of the dislocations is indicated by b and an arrow.

grain interior and near the GBs, unlike what was observed in a fatigued nanotwin Cu film [31]. The cyclic deformation-induced threading dislocation arrays are spread unevenly in the interiors of twin channels with a spacing from 100 to 1000 nm, which is comparable to the size of the blocks along the TBs (Fig. 5d) and the spacing of "zigzag" slip bands (Figs. 5c and 6a and b).

The high-magnification TEM images in Fig. 9b reveal that the threading dislocation lines are confined by a few neighboring twin lamellar channels, which are analogous to the hairpin threading dislocations observed in nanoscale thin films and multilayer materials [15,18,50–52]. Fewer dislocation locks or tangles are found inside the twin lamellae. For grains undergoing a large cumulative cyclic strain, a large number of threading dislocation arrays propagating in the twin lamella are present in bundles, which result in the "zigzag" slip bands in col-nt-Cu (Fig. 5). Both the threading bundles and the fewer dislocation locks/tangles in the twin lamellae would lessen the stress concentration in the grains and ultimately improve the fatigue life.

During tension–tension fatigue testing, the threading dislocation usually initiates at the sample surface or at GBs, propagates in the grain interior through a long twin lamellar channel and finally piles up against the opposite side of the GBs. GBs could act either as dislocation sources or as dislocation sinks and sustain a large of cyclic plastic strains. When the stress/strain concentration at a GB is too large to be compatible, a crack will nucleate there, as seen in Fig. 7.

Another interesting finding is that most of the slip morphologies on the top surface have an angle of 45° relative to the loading axis in col-nt-Cu (Fig. 4b). Similarly, slip band traces with an angle of 45° relative to the loading axis are also frequently seen on the top surface (the (1 1 1) plane) of fatigued single-crystal Cu [46,53]. Theoretically, there are no traces of slip bands left on the top surface when the Burgers vector of the slip band-related dislocations are strictly parallel to the loading axis. However, marked traces with a typical 45° relative to the loading axis can be found occasionally, when the top surface is slightly off the (1 1 1) orientation. For col-nt-Cu, the Schmid factor calculation shows that the maximum Schmid factor $\sqrt{2}/3$ can be achieved only when the Burgers vector is at an angle of 45° relative to the loading axis. Threading dislocations can be easily and preferentially active in a few columnar grains with some specific in-plane orientations, as shown in Fig. 8. Similar to the case of the fatigued single Cu described above, theoretically, no surface slip traces appear on the top surface of col-nt-Cu. However, if the out-of-plane orientation of some grains with the maximum Schmid factor $\sqrt{2}/3$ is slightly off the (1 1 1) plane, 45° surface traces would appear in some grains on the top surface. This analysis can also rationalize why the typical "zigzag" slip bands can only be activated in some columnar grains, as indicated from the cross-section view in Fig. 5a. Fig. 10 presents an overall 3-D illustration of the plane-view traces of the slip bands and zigzag slip bands from a cross-section of the fatigued col-nt-Cu sample. Such uniform threading dislocations with a hard mode II single slip system confined

within nanoscale twin channels, giving rise to "zigzag" slip bands on the cross-section surface and typical slip traces on the top surface, is fundamentally different from the extrusion morphology appearing in the twin-free polycrystalline Cu [35,47–49].

Besides the TB orientation with respect to the loading orientation, the cyclic deformation behavior of col-nt-Cu is heavily influenced by the twin thickness and grain size. If the twin spacing is too thick to confine other slip systems, secondary or multiple slip systems with a smaller Schmid factor could be activated at a relatively high stress. Only at the nanometer scale could the twin lamella be an effective barrier for dislocation bowing out, as shown in Fig. 8c. The severely confined uniform threading dislocations inside the twin lamellae at nanometer scale restrict the annihilation and rearrangement of dislocations to form PSBs, like those which appear in CG-Cu [41,54]. Guo et al. [55] studied the twin thickness effect on the dislocation morphologies of pure Cu under fatigue tests. They showed that no PSB structures are formed when the twin thickness is less than 1 μm. In the present tension–tension fatigue tests, only threading dislocations gliding in one direction in a single twin channel are observed. It is thus not easy to form dislocation dipoles, the important component for PSB formation, in nanoscale twin interiors. As discussed previously, only one set of primary slip systems is activated in columnar grains with highly oriented nanoscale twins. Thus the cyclic deformation of the col-nt-Cu sample is more like that in a fatigued "quasi-single" crystal material than that in a fatigued common polycrystal structure. Meanwhile, the secondary slip cannot be activated due to the confinement of the nanoscale twins, so cell or labyrinth structures consisting of more than one slip system related dislocation also will not be produced in col-nt-Cu samples.

The grain size, i.e. the twin lamellar length, also exhibits a strong influence on the mechanical behavior of col-nt-Cu.

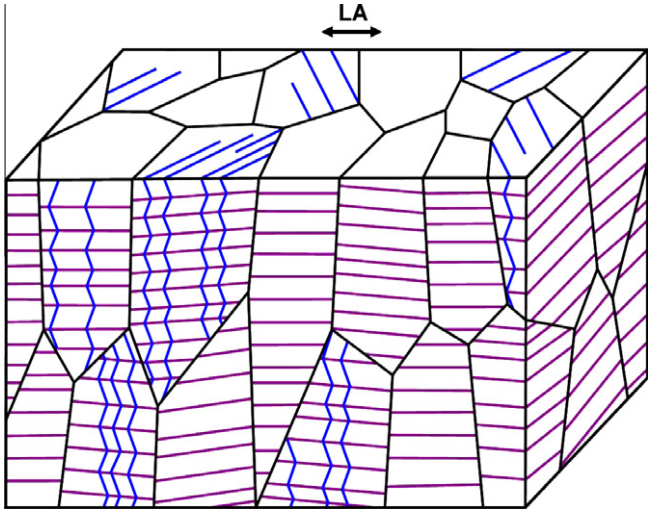

Fig. 10. Schematic illustration of surface fatigue features for col-nt-Cu sample, i.e. traces of slip bands at 45° relative to cyclic loading axis from the *A* direction and "zigzag" slip bands crossing TBs from the *B* direction in some columnar grains.

An obvious uniform strain (>2%) can only be identified for col-nt-Cu with $d > 3$ μm, in despite of the presence of high-density TBs [18]. This is because sub-micron-sized grains suppress lattice dislocation activity, which results in limited work hardening in the grain interior. Shute et al. [30,31] found that a substantial volume of grains lose their original twin structure and detwinned regions are prevalently observed around GB regimes in the fatigued UFG-Cu samples containing highly aligned nanotwins. In contrast, in the present study with micrometer-size grained nt-Cu, the larger grain size provides sufficient room for confined threading dislocations to propagate individually from one side of a GB to the other.

5. Conclusion

The fatigue life of bulk micrometer-sized columnar-grained Cu samples with preferentially oriented nanoscale twins is significantly enhanced in comparison with that of CG-Cu with essential similar grain size. The fatigue limit ($\sigma_{max} = 162$ MPa at 10^7) of columnar-grained nt-Cu is greatly improved over that of CG-Cu. The cyclic deformation of the polycrystalline columnar-grained Cu with nanoscale twins resembles that in a fatigued "quasi-single" crystal metal, where only one set of primary slip systems with the slip Burgers vector parallel to TBs but the slip plane inclined to TBs (namely the threading dislocation) is preferentially activated when the cyclic loading direction is parallel to the twin planes. Such uniform threading dislocations with a single slip system confined within nanoscale twin channels give rise to "zigzag" slip bands crossing a few TBs, which is fundamentally different from extrusion morphology that appears in conventional CG-Cu. The nanoscale twin confinement of activated threading dislocation bundles and the fewer dislocation locks/tangles in the twin lamellae lessen the stress concentration in the grains and contribute to the enhanced fatigue limit and fatigue life of col-nt-Cu.

Acknowledgements

The authors acknowledge the financial support from the National Science Foundation of China (Grant Nos. 50890171, 50911130230 and 51071153), the National Basic Research Program of China (973 Program, 2012CB932202), the MOST International S&T Cooperation project of China (2010DFB54010), the "Hundred of Talents Project" of the Chinese Academy of Sciences (CAS). The authors are grateful to Profs. H. Mughrabi, S.X. Li, Z.F. Zhang, D. Embury and Y. Brechet for stimulating discussions and Mr. S. Jin for nanotwin Cu samples preparation.

References

[1] Koch CC, Morris DG, Lu K, Inoue A. MRS Bull 1999;24:54.
[2] Gleiter H. Acta Mater 2000;48:1.

[3] Kumar KS, Van Swygenhoven H, Suresh S. Acta Mater 2003;51:5743.
[4] Meyers MA, Mishra A, Benson DJ. Prog Mater Sci 2006;51:427.
[5] Lu K, Lu L, Suresh S. Science 2009;324:349.
[6] Agnew SR, Vinogradov AY, Hashimoto S, Weertman JR. J Electron Mater 1999;28:1038.
[7] Hanlon T, Kwon YN, Suresh S. Scripta Mater 2003;49:675.
[8] Mughrabi H, Höppel HW, Kautz M. Scripta Mater 2004;51:807.
[9] Kunz L, Lukas P, Svoboda A. Mater Sci Eng, A 2006;424:97.
[10] Zhang K, Weertman JR. Metall Mater Trans A 2009;40A:2255.
[11] Wu SD, Wang ZG, Jiang CB, Li GY, Alexandrov IV, Valiev RZ. Scripta Mater 2003;48:1605.
[12] Lu L, Shen YF, Chen XH, Qian LH, Lu K. Science 2004;304:422.
[13] Shen YF, Lu L, Lu QH, Jin ZH, Lu K. Scripta Mater 2005;52:989.
[14] Lu L, Dao M, Zhu T, Li J. Scripta Mater 2009;60:1062.
[15] Lu L, You ZS, Lu K. Scripta Mater 2012;66:837.
[16] Dao M, Lu L, Shen YF, Suresh S. Acta Mater 2006;54:5421.
[17] Zhu T, Gao H. Scripta Mater 2012;66:843.
[18] You ZS, Lu L, Lu K. Acta Mater 2011;59:6927.
[19] Asaro RJ, Suresh S. Acta Mater 2005;53:3369.
[20] Zhu T, Li J, Samanta A, Kim HG, Suresh S. Proc Natl Acad Sci USA 2007;104:3031.
[21] Jin ZH, Gumbsch P, Albe K, Ma E, Lu K, Gleiter H, et al. Acta Mater 2008;56:1126.
[22] Kulkarni Y, Asaro RJ. Acta Mater 2009;57:4835.
[23] Shabib I, Miller RE. Acta Mater 2009;57:4364.
[24] Li XY, Wei YJ, Lu L, Lu K, Gao HJ. Nature 2010;464:877.
[25] Thompson N. In: Averbach BL, Felbeck DK, Hahn JT, Thomas DSE, editors. Fracture, proceedings of the international conference on atomic mechanisms of fracture. London: Chapman & Hall; 1959.
[26] Neumann P, Tonnessen A. In: Kettunen PO, Lepisto TK, Lehtonen ME, editors. Strength of metals and alloys. Oxford: Pergamon; 1988.
[27] Heinz A, Neumann P. Acta Metall Mater 1990;38:1933.
[28] Qu S, Zhang P, Wu SD, Zang QS, Zhang ZF. Scripta Mater 2008;59:1131.
[29] Zhang ZJ, Zhang P, Li LL, Zhang ZF. Acta Mater 2012;60:3113.
[30] Shute CJ, Myers BD, Xie S, Barbee TW, Hodge AM, Weertman JR. Scripta Mater 2009;60:1073.
[31] Shute CJ, Myers BD, Xie S, Li SY, Barbee Jr TW, Hodge AM, et al. Acta Mater 2011;59:4569.
[32] Tang L, Lu L. Acta Metall Sin 2009;45:808.
[33] Singh A, Tang L, Dao M, Lu L, Suresh S. Acta Mater 2011;59:2437.
[34] Lee YL, Pan L, Hathaway RB, Barkey ME. Fatigue testing and analysis: theory and practice. Burlington (VT): Elsevier; 2005.
[35] Mughrabi H, Wang R, Differt K, Essmann U. ASTM Spec Tech Pub 1983;811:5.
[36] Wang Z, Laird C. Mater Sci Eng 1988;100:57.
[37] Bayerlein M, Mughrabi H. Acta Metall Mater 1991;39:1645.
[38] Cretegny L, Saxena A. Acta Mater 2001;49:3755.
[39] Ma J. Mater Sci Eng, A 2007;457:63.
[40] Mughrabi H, Bayerlein M, Wang R. In: Brandon DG, Chaim R, Rosen A, Freund LB, editors. Strength of metals and alloys. London: Freund; 1991.
[41] Winter AT, Pedersen OR, Rasmussen KV. Acta Metall 1981;29:735.
[42] Polák J, Klesnil M. Mater Sci Eng 1984;63:189.
[43] Wang R, Mughrabi H. Mater Sci Eng 1984;63:147.
[44] Liu CD, Bassim MN, You DX. Acta Metall Mater 1994;42:3695.
[45] Mughrabi H, Ackermann F, Herz K. ASTM Spec Tech Pub 1979;675:68.
[46] Basinski ZS, Basinski SJ. Prog Mater Sci 1992;36:89.
[47] Essmann U, Gosele U, Mughrabi H. Philos Mag A 1981;44:405.
[48] Differt K, Esmann U, Mughrabi H. Philos Mag A 1986;54:237.
[49] Mughrabi H. Metall Mater Trans B 2009;40:431.
[50] Freund LB. J Appl Mech 1987;54:553.
[51] Nix W. Metall Trans A 1989;20:2217.
[52] Misra A, Hirth JP, Hoagland RG. Acta Mater 2005;53:4817.
[53] Basinski ZS, Basinski SJ. Acta Metall 1989;37:3263.
[54] Suresh S. Fatigue of materials. 2nd ed. Cambridge: Cambridge University Press; 1998.
[55] Guo XL, Lu L, Li SX. Acta Metall Sin 2005;41:23.